bioRxiv preprint doi: https://doi.org/10.1101/2020.05.05.078410; this version posted May 5, 2020. The copyright holder for this preprint (which was not certified by peer review) is the author/funder. All rights reserved. No reuse allowed without permission.

Novel strategies of Raman imaging for monitoring intracellular retinoid metabolism in cancer cells

Short title: Raman imaging to monitor retinoid metabolism in cancer cells

Halina Abramczyk [1,*], Anna Imiela [1] and Jakub Surmacki [1]

[1] Lodz University of Technology, Faculty of Chemistry, Institute of Applied Radiation Chemistry, Laboratory of Laser Molecular Spectroscopy, Wroblewskiego 15, 93-590 Lodz, Poland; halina.abramczyk@p.lodz.pl, anna.imiela@p.lodz.pl, jakub.surmacki@p.lodz.pl

* Correspondence: halina.abramczyk@p.lodz.pl ; Tel.: +48426313188 (H.A.)

Abstract: We developed a label-free Raman method for whole-cell biochemical imaging to detect molecular processes that occur in normal and cancer brain cells due to retinol transport in human cancers at the level of isolated organelles. Our approach allows the creation of biochemical maps of lipid droplets, mitochondria and nuclei in single cells. The maps were capable of discriminating triglycerides (TAG) from retinyl ester (RE) in lipid droplets (LD), providing an excellent tool to monitor intracellular retinoid metabolism. We detected spectral changes that arose in proteins and lipids due to retinoid metabolism in human cell lines of normal astrocytes and high-grade cancer cells of glioblastoma as well as in human medulloblastoma and glioblastoma tissue. Raman imaging is an effective tool for monitoring of retinoids and retinol binding proteins involved in carcinogenesis, as monitored by the unique spectral signatures of vibrations. We found two functionally distinct lipid droplets: TAG-LD, for energy storage, and RE-LD, for regulating the level of apo-CRBP1 in cytosol. Raman polarization measurements revealed the occurrence of conformational changes affecting discrete regions of proteins associated with retinol binding. Aberrant expression of retinoids and retinol binding proteins in human tumours were localized in lipid droplets, mitochondria and nuclei according Raman imaging.

Keywords: Raman spectroscopy; Raman imaging; U-87 MG cell lines; astrocytes; brain cancer; glioblastoma; phosphorylation; retinoids; retinol binding protein

Abbreviations: apo-CRBP1, apo-cellular retinol-binding protein-I; ATP, adenosine triphosphate; CRBP-1, cellular retinol-binding protein-I; JAK, Janus kinase; LD, lipid droplets; MRI, magnetic resonance imaging; NHA, normal astrocytes (CC-2565, Lonza); OA, oleic acid; PKC delta, protein kinase C delta; RA, retinoic acid; RBP, retinol binding protein; RE, Retinyl ester; RI, Raman imaging; ROL, retinol; RP, retinyl palmitate; STAT, signal transducer and activator of transcription; STRA6, stimulated by retinoic acid 6; TAG, trigyceride as glyceryl tripalmitate; U-87 MG, high-grade cancer cells of human glioblastoma (HTB-14, ATCC)

bioRxiv preprint doi: https://doi.org/10.1101/2020.05.05.078410; this version posted May 5, 2020. The copyright holder for this preprint (which was not certified by peer review) is the author/funder. All rights reserved. No reuse allowed without permission.

Introduction

Vitamin A plays multiple functions in a wide range of biological processes including cell differentiation, proliferation, and apoptosis. Recent results analysed in the context of a number of literature studies suggest that processes that occur in carotenoids and retinoids play an important role in the molecular mechanisms of carcinogenesis.[1–5]

In the past, considerable effort has been directed towards the cancer chemoprevention properties of carotenoids and retinoids[6,7], but relatively little attention has been paid to their role in molecular mechanisms of cancer development. Although effort has been focused almost exclusively on their antioxidant activity, their biological activity goes far beyond this signature, and a careful examination of other possible involvements in metabolism and signaling of cells is needed. It has recently been reported that carotenoid expression is one of the most common abnormalities in human cancers. Carotenoid expression is lower in human cancers than in normal cells.[8–10] In recent years, data have emerged indicating a role of retinoids in lipid droplets.[11] It has recently been reported that retinyl esters are replaced by polyunsaturated triacylglycerol species in lipid droplets of hepatic stellate cells during activation.[11]

Carotenoids are delivered to the human body via the diet because they are present in a wide range of vegetables and fruits.[12] Some carotenoids (β-carotene, α-carotene and β-cryptoxanthin) belong to the family of provitamin A carotenoids because they are precursors of vitamin A, a fat-soluble retinol.[13] Beta-carotene is transformed into vitamin A by cleavage into the all-trans retinol form (one of the major forms of vitamin A) within the small intestine when retinol is absorbed. The transformation of beta-carotene is catalysed by the enzyme β-carotene dioxygenase in the small intestine (intestinal mucosa) to form retinal, followed by retinal reduction to retinol by retinaldehyde reductase in the intestine.

Vitamin A is also delivered directly as preformed vitamin A, which is naturally present in food of animal origin such as meat, fish, and dairy products[14], consisting primarily of retinyl palmitate (fatty acid ester), and retinol, and in much smaller concentrations as retinoic acid. The preformed vitamin A is provided in food of animal origin via the absorption of retinol from the alimentary tract accompanied by the absorption of other food molecules. The retinol conjugates to some of the absorbed molecules, particularly fatty acids to form esters such as retinyl palmitate, which is also converted to retinol within the lumen of the small intestine and then re-esterified to form retinyl ester within the enterocyte.[15] After the conversion of carotenoids and retinal esters, retinol is transported through the lymphatic or blood circulation to other cells and tissues where it binds to retinol-binding proteins (RBP) in the liver, controlling the release of retinol from storage when it is needed.[16–18] A large number of physiological processes, such as vision, epithelial differentiation in cancers, inflammatory processes, and spermatogenesis, are attributed to vitamin A.[19–30]

The involvement of vitamin A in processes of vision is its most well-known characteristic, but other mechanisms linked to vitamin A are much less well understood and await further investigation. The relationship between retinoids and cancer has been reported in many studies.[1,25,31] Several studies using animal models have reported an inhibitory role of retinoids in breast cancer.[1,23] Lower expression of cellular retinol-binding protein-I (CRBP-1) has been found in breast and other human cancers, but its significance is not well understood.[1] It has been reported that retinoids can be used in the treatment of glioma.[31] Alterations in cellular binding protein expression modify retinoid biological functions and result in abnormal glucose and energy metabolism, thus increasing the predisposition to breast cancer, prostate cancer, ovarian adenocarcinoma, and glioblastoma.[32] Vitamin A has been reported to control oxidative phosphorylation in mitochondria.[33] As is well known, the most universal feature of cancer is a high rate of glucose uptake and enhanced glycolytic activities followed by lactate fermentation known as the Warburg effect.[34] Understanding the mechanism of altered energy metabolism that replaces the more efficient oxidative phosphorylation in terms of the yield of adenosine triphosphate (ATP) with the less efficient glycolysis represents the pivotal problem that must be solved for progress in eliminating cancer. During the past decade, many studies have suggested that the metabolic fate of pyruvate is regulated by tyrosine phosphorylation.[35]

bioRxiv preprint doi: https://doi.org/10.1101/2020.05.05.078410; this version posted May 5, 2020. The copyright holder for this preprint (which was not certified by peer review) is the author/funder. All rights reserved. No reuse allowed without permission.

Vitamin A plays an important role in cell signaling. Abnormal retinoid signaling in the cytoplasm and nucleus has been reported in human cancers.[36] Vitamin A is involved in cell signaling by attachment to the retinol-binding protein receptor termed STRA6 (stimulated by retinoic acid 6).[37] STRA6 is a transmembrane cell surface protein that functions as a receptor for a family of retinol-binding proteins (RBPs) that play roles as carrier proteins that bind to retinol.[2,38] STRA6 is a ligand-activated cell surface signaling receptor that, upon binding of the retinol-RBP complex (also termed the holo-RBP or RBP-ROH complex) activates JAK/STAT signaling to transfer information from the extracellular environment to the nucleus, resulting in DNA transcription and inducing the expression of target genes involved in many processes such as immunity, proliferation, differentiation, and apoptosis. Disrupted JAK/STAT signaling may lead to a variety of diseases, such as cancers and disorders of the immune system.[39] Janus kinases (JAKs) belong to an enzyme family of intracellular, nonreceptor tyrosine kinases that activate STAT signaling. STAT (signal transducer and activator of transcription) is a member of protein family that activates genes through transcription. The transport of retinol to the interior of the cell occurs via the retinol acceptor CRBP1 protein attached to the CRBP binding loop of STRA6. This event activates the intracellular non-receptor tyrosine kinase enzyme JAK2, which transfers a phosphate group from ATP to a protein in the cell, thereby phosphorylating STRA6 at Y643 (tyrosine).[2] The detailed mechanism of JAK2 activation by the retinol-RBP complex is still unknown and awaits further investigation to elucidate the cascade of downstream signals and events necessary to activate (or suppress) gene transcription in the nucleus.

To avoid the pitfalls of conventional approaches and to obtain biochemical information in a realistically crowded biological environment, it is necessary to develop new tools for the precise analysis of signals from molecules present in specific organelles of cells: proteins, fatty acids and lipids, DNA, RNA, carbohydrates, carotenoids, retinoids, and primary metabolites, which can be obtained by Raman microscopy.

Raman microspectroscopy - a spectroscopic technique based on inelastic scattering of monochromatic light - does not require labelling of the molecules of interest and enables direct specific chemical imaging of biomolecules such as DNA/RNA, proteins, and lipids in intact cells and tissues.[40–42]

We will show that label-free Raman microscopy could also enable the clarification of the precise role of retinoids in the metabolism and signaling of cancer cells. The purpose of this paper is to examine the role of carotenoids, vitamin A, and retinoids in human cell lines of normal astrocytes (NHA) and high-grade cancer cells of glioblastoma (U-87 MG) and in human medulloblastoma and glioblastoma tissues.

This paper provides a basis for substantial revision of the previous interpretation of the biochemical events associated with retinol in normal and cancer cells. We hope that the present contribution will facilitate experimental endeavours in molecular biology and spectroscopy to fully understand the role of retinol in transport, metabolism and signaling in carcinogenesis. It is reasonable to speculate that pharmacologically enhanced carotenoids and retinol activity may represent a possible method to inhibit certain types of cancer.

Results

Here we will focus on information that can be extracted from Raman microscopy and Raman imaging of human central nervous system tissue from astrocytoma and medulloblastoma, as well as cell lines of normal human astrocytes (NHA), and glioblastoma (U-87 MG) cells. We will focus on cellular organelles such as the nucleus, lipid droplets, and mitochondria of NHA and U-87 MG cells.

Figure 1 shows a typical Raman image and Raman spectra of central nervous system tissue from medulloblastoma and pilomyxoid astrocytoma compared with a white light microscopy image and MRI image. MRI provides the primary clinical information concerning the localization of the pathology, but Figure 1 shows that MRI has significantly limited spatial resolution in comparison to the Raman image. The Raman image offers unsurpassed spatial resolution combined with excellent spectral resolution. Therefore, Raman imaging is much more than simple microscopy because the Raman spectra embedded

bioRxiv preprint doi: https://doi.org/10.1101/2020.05.05.078410; this version posted May 5, 2020. The copyright holder for this preprint (which was not certified by peer review) is the author/funder. All rights reserved. No reuse allowed without permission.

in the tissue image provide information about the biochemical composition of brain tissue with lipid-rich, protein-rich and mixed profiles, which are characteristic of brain white matter, tumours, and cortex with cellular, myelin-rich regions.[40,43–45]

The different Raman profiles of specific brain regions presented in Figure 1 reflect the different compositions of lipid-rich and protein-rich regions. The red and blue areas in Figure 1 reflect the locations of proteins and lipids in specific brain regions, respectively. We have identified the Raman vibration profiles in our previous papers.[40,42,43,46]

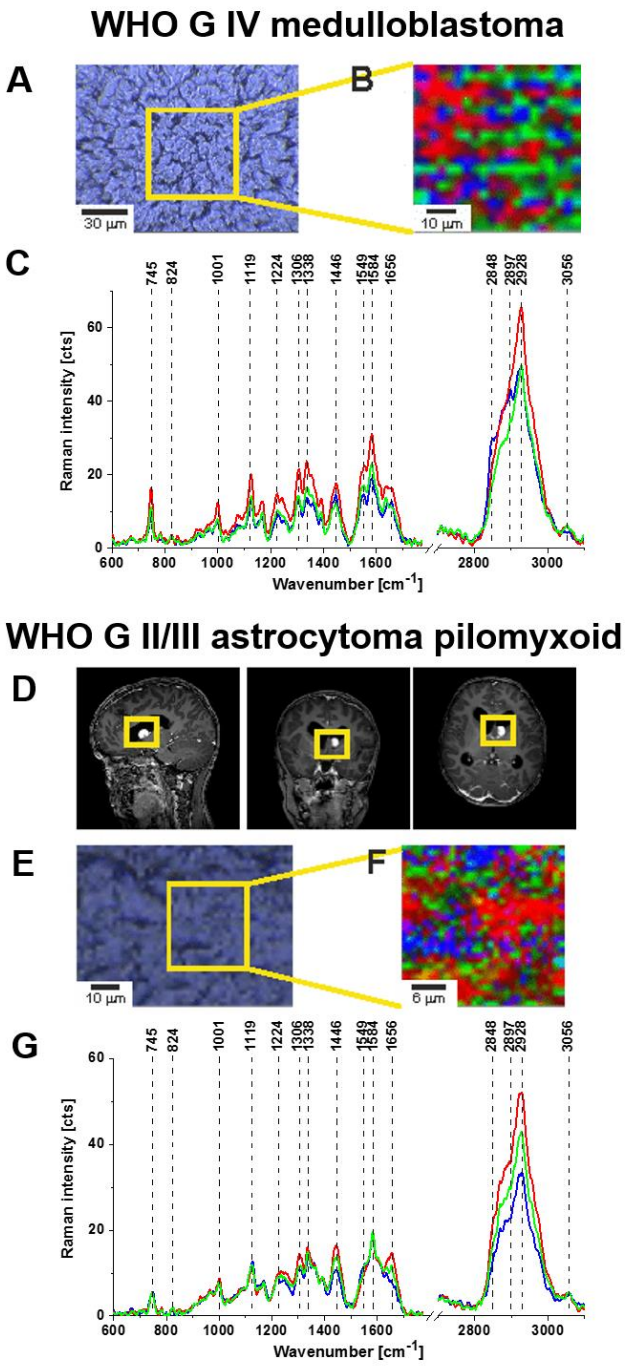

Figure 1. Raman spectroscopy analysis of medulloblastoma and astrocytoma. Microscopy image (A), Raman image (B), and characteristic Raman spectra (C) of WHO G IV medulloblastoma (P49). MRI images (D), microscopy image (E), Raman image (F) and characteristic Raman spectra (G) of WHO G II/III pilomyxoid astrocytoma (P51). The integration time for the Raman images was 0.5 s with a resolution step of 1 µm per 1 pixel, laser: 532 nm excitation, power: 10 mW. The line colours of the spectra correspond to the colours of the Raman maps. The Raman maps were generated using basis analysis.

bioRxiv preprint doi: https://doi.org/10.1101/2020.05.05.078410; this version posted May 5, 2020. The copyright holder for this preprint (which was not certified by peer review) is the author/funder. All rights reserved. No reuse allowed without permission.

Numerous marked differences are apparent between the protein-rich and lipid-rich regions. The most significant differences are observed at 1584 cm^{-1} and 1656 cm^{-1} corresponding to amide II and amide I vibrations, respectively.

To evaluate Raman imaging as a diagnostic tool for identifying tumours based on the biochemical composition of specific brain regions, one must better understand the differences presented in Figure 1. Thus, we compared the Raman spectra of the brain tumour tissue using different laser excitation wavelengths. This approach can reduce fluorescence at higher excitation wavelengths and might generate Raman resonance enhancement at lower excitation wavelengths for some tissue components that are visible for non-resonance conditions.

Figure 2 shows the Raman spectra of the high-grade medulloblastoma and low-grade astrocytoma tissues at an excitation wavelength of 785 nm, 532 nm, and 355 nm and different polarization configurations. The different excitations were sensitive to the selective resonance Raman enhancement and fluorescence of the chromophores attached to the proteins and lipids. Polarized Raman spectroscopy can provide information about molecular symmetry and orientation as well as the symmetry of the bond vibrations, resulting in better visualization of the cancerous and normal tissue structures. The different polarization configurations reflect the conformational modifications of the proteins and lipids. As the Raman absorption resonance of both forms were similar, the modification of protein structures clearly must depend on the chromophore attached to the proteins or lipids that alter the resonance conditions.

Dramatic differences can be observed due to the excitation as well as the polarization configurations in the Raman spectra for vibrations corresponding both to lipids and proteins. The most significant differences were observed at 1584 cm^{-1} and 1656 cm^{-1} corresponding to corresponding to amide II and amide I vibrations, respectively. Figure 2 shows that the Raman intensity of the band of amide I at 1656 cm^{-1} at 785 nm increased in tumour tissue compared with 355 and 532 nm. By contrast, the Raman intensity of the band at 1584 cm^{-1} increased at 355 nm and 532 nm and diminished at 785 mn, indicating that the chromophore attached to the protein is absorbed in the range from 355-532 nm. The identification of the chromophore will be discussed in detail later in the paper.

bioRxiv preprint doi: https://doi.org/10.1101/2020.05.05.078410; this version posted May 5, 2020. The copyright holder for this preprint (which was not certified by peer review) is the author/funder. All rights reserved. No reuse allowed without permission.

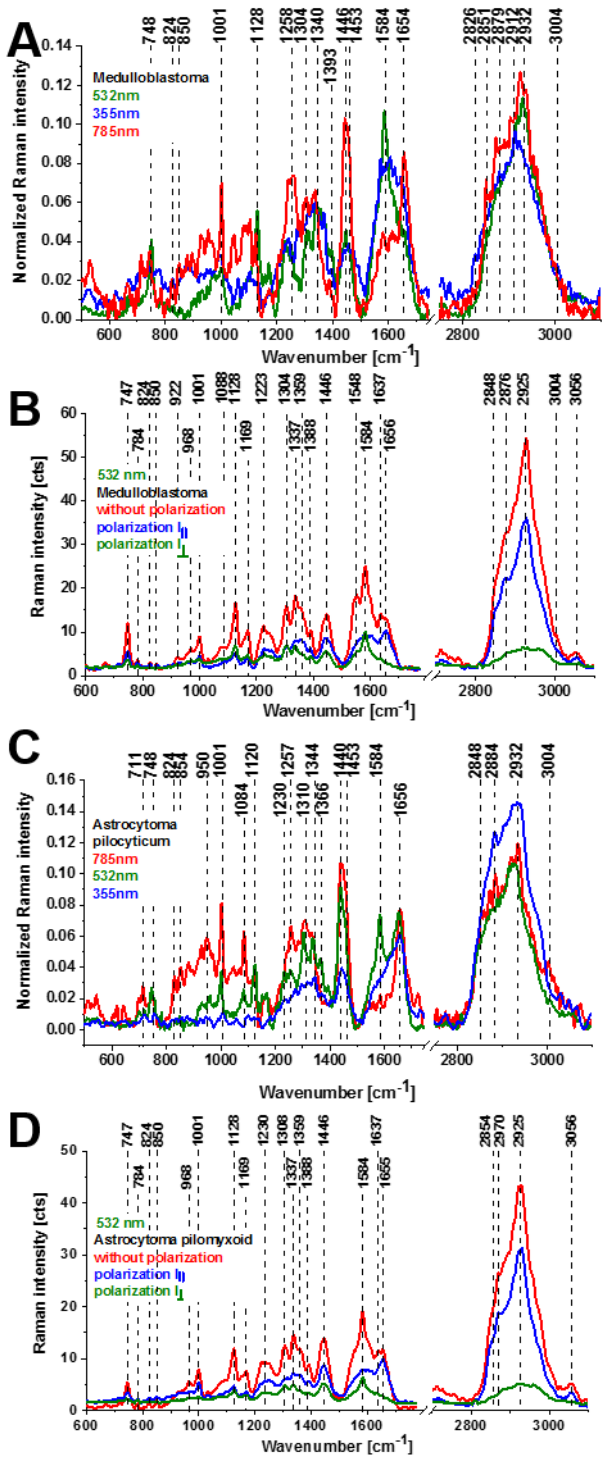

Figure 2. Raman vector normalized average spectra of human brain tissue from medulloblastoma (grade IV) (A), and astrocytoma (pilocyticum, grade I) (C) at 785 nm, 532 nm, and 355 nm wavelength excitation. Raman spectra for different polarization configurations at 532 nm: medulloblastoma (grade IV) (non-polarized Raman signal (red), parallel polarization $I_{\parallel}$ (blue), perpendicular polarization $I_{\perp}$ (green)) (B), and pilomyxoid astrocytoma (non-polarized Raman signal (red), parallel polarization $I_{\parallel}$ (blue), perpendicular polarization $I_{\perp}$ (green)) (D). Raman spectra in (B) and (D) were acquired at 0.5 s and 10 accumulations.

The results obtained for different polarization configurations showed that the Raman signal at 1656 cm^{-1} reflecting vibrations of the α-helix protein structure under parallel polarization became weaker

bioRxiv preprint doi: https://doi.org/10.1101/2020.05.05.078410; this version posted May 5, 2020. The copyright holder for this preprint (which was not certified by peer review) is the author/funder. All rights reserved. No reuse allowed without permission.

under perpendicular polarization of the excitation and scattered beams. By contrast, the Raman signal at 1584 cm^{-1} that reflects vibrations of the β-sheet structure was significantly enhanced under perpendicular polarization of the excitation and scattered beams. The origin of the protein that is related to the band 1584 cm^{-1} will be discussed later.

The second spectral region with notable differences in the Raman signal for various excitations was attributed to the presence of lipids at approximately 1437-1444 cm^{-1} (fatty acids, triglycerides, CH_2 or CH_3 deformation modes[46,47]), 1742 cm^{-1} (C=O stretching), proteins at 1453 cm^{-1} (proteins[47,48] C-H wag, CH_2 or CH_3 def.) and ~2845-2940 cm^{-1} (CH_2, CH_3 stretching of lipids and proteins).

Figure 2 shows the average Raman spectra providing information on the global amount of lipids and proteins in human brain tissue from medulloblastoma and astrocytoma. To gain information about the chemical composition of specific organelles such as lipid droplets, the nucleus, mitochondria, and the cytoplasm inside the cells, we must focus our attention on individual cells.

Figure 3 shows Raman images of glioblastoma cells (U-87 MG) compared with fluorescence images of dyes which specifically label different cellular organelles: Hoechst 33342, Oil Red O, and Mitotracker Red CMXROS labelling the nucleus (red labeled), lipid droplets (blue labeled), and mitochondria (magenta labeled), respectively.

bioRxiv preprint doi: https://doi.org/10.1101/2020.05.05.078410; this version posted May 5, 2020. The copyright holder for this preprint (which was not certified by peer review) is the author/funder. All rights reserved. No reuse allowed without permission.

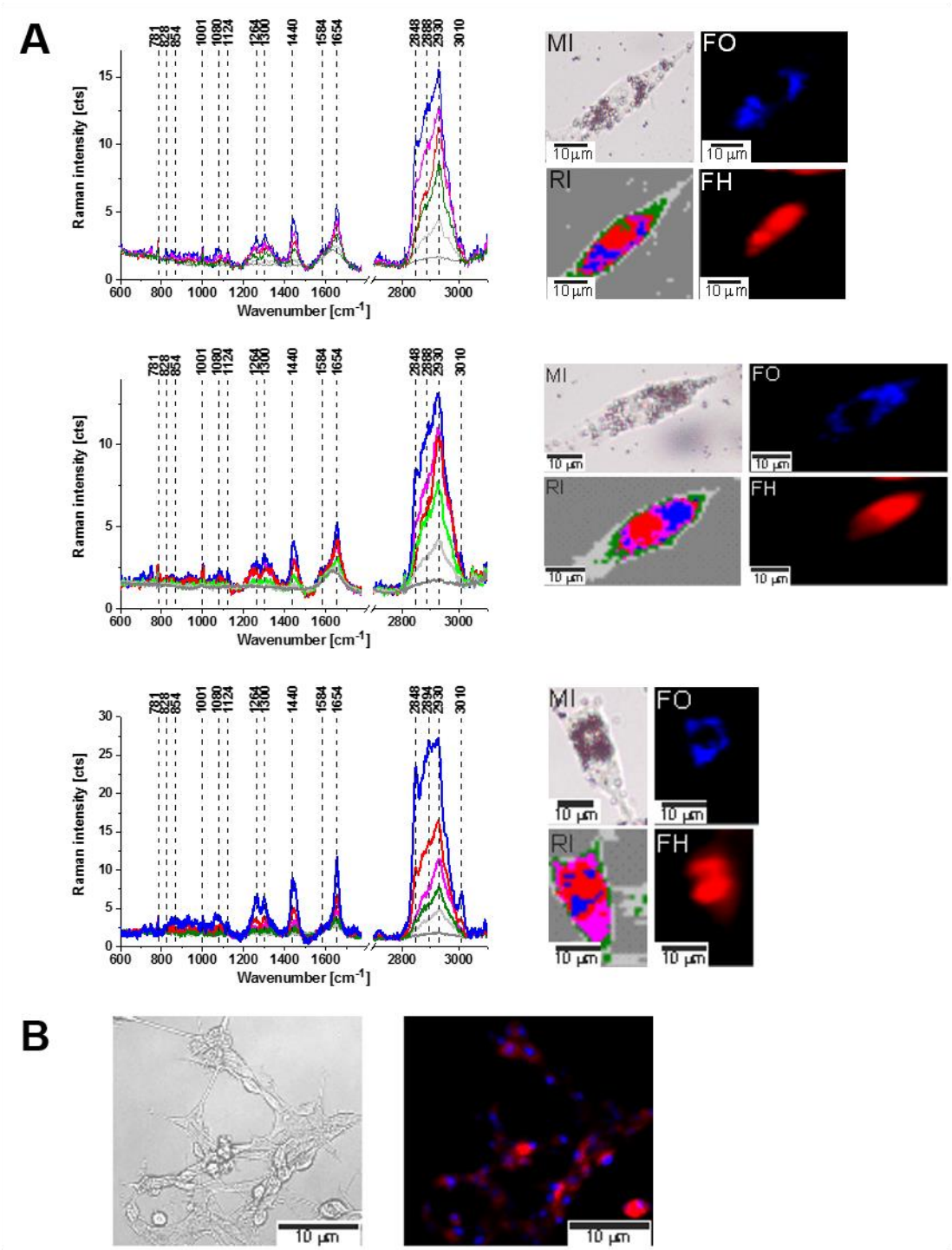

Figure 3. Confocal Raman spectroscopy analysis of the glioblastoma (U-87 MG) cell line at the 532 nm wavelength excitation (A) (Raman cluster spectra of nucleus (red), lipid droplets (blue), cytoplasm (green), mitochondria (magenta), cell border (light grey), area out of cell (dark grey), Raman cluster image (RI), microscopy image after Oil Red O staining (MI), fluorescence image of Oil Red O staining (FO), and fluorescence image of Hoechst 33342 staining (FH). Microscopy and fluorescence image of U-87 MG cells stained with Mitotracker Red CMXROS and Hoechst 33342 (B).

The complete spectral and microscopic identification of organelles in normal and cancer cells allowed us to analyse the biochemical composition of lipid droplets, the nucleus and mitochondria by Raman mapping of cellular compartments.

bioRxiv preprint doi: https://doi.org/10.1101/2020.05.05.078410; this version posted May 5, 2020. The copyright holder for this preprint (which was not certified by peer review) is the author/funder. All rights reserved. No reuse allowed without permission.

First, we will focus on lipid droplets because Figure 3 MI (Oile Red O staining) and Figure 3 RI (Raman imaging) show a large concentration of lipid droplets around the nucleous. We want to check whether this feature is characteristic for highly aggressive cancers such as glioblastoma or it is also typical also for normal glial cells. Recently, we have found that the main components of lipid droplets are esters of glycerol and fatty acids - triacylglycerols (TAG), which are related mainly to their function as energy storage deposits.[42]

Here, we will concentrate on other important functions of lipid droplets, particularly cell signaling, which are related to commonly neglected in the past alterations in accumulation of retinoids in lipid droplets. Recent research has revealed exciting new aspects of retinoids importance in the regulation of lipid metabolism, cell signaling, membrane trafficking and control of the synthesis and secretion of inflammatory mediators.[49]

We will examine in detail differences in chemical composition of lipid droplets, mitochondria and nucleous in normal astrocytes and high-grade malignant human brain cells (glioblastoma).

First, we assessed the impact of cancer aggressiveness on the amount of cytosolic lipid droplets. Figure 4 show the microscope images, Raman images, and fluorescence images of normal human astrocytes (NHA) and high-grade glioblastoma cells (U-87 MG) compared with images of lipid droplets stained with Oil Red O dye.

bioRxiv preprint doi: https://doi.org/10.1101/2020.05.05.078410; this version posted May 5, 2020. The copyright holder for this preprint (which was not certified by peer review) is the author/funder. All rights reserved. No reuse allowed without permission.

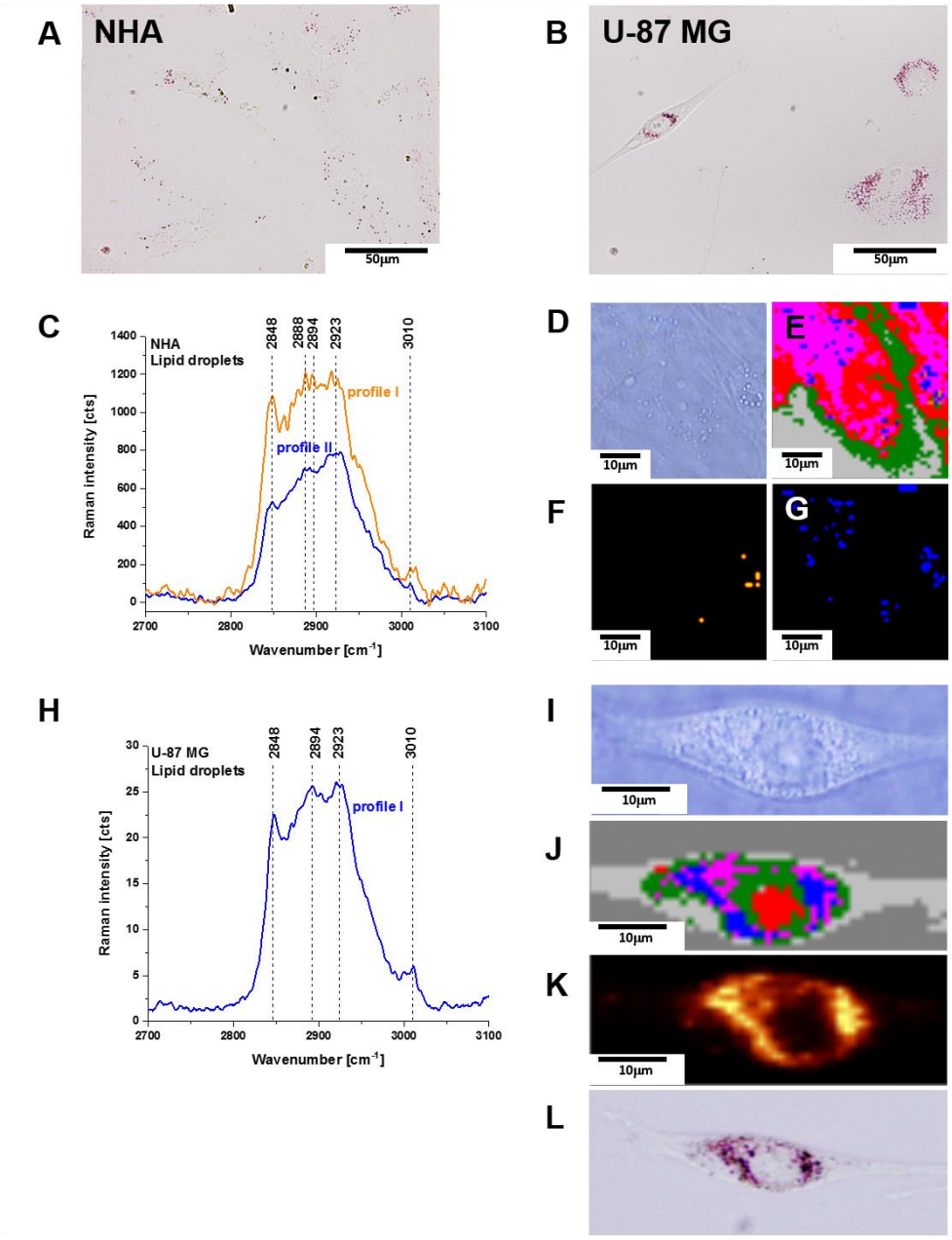

Figure 4. Microscopy images of lipid droplets stained with Oil Red O dye in normal human astrocytes (A) and high-grade glioblastoma U-87 MG (B and L), Raman spectra of lipid droplets of normal astrocytes, profile I – TAG (orange), profile II – retinyl esters (blue) (C), microscopy image (D), Raman cluster image (E) and Raman image of the distribution of lipid droplets with profile I (F) and profile II (G) in NHA. Average Raman spectrum of lipid droplets obtained from cluster analysis (H), microscopy image (I), Raman cluster image (J) and fluorescence image of Oil Red O (K) and microscopy images of Oil Red O-stained lipid droplets (L) of U-87 MG high-grade glioblastoma. Raman analysis were performed at 532 nm laser excitation. Nucleus was labeled by red, lipid droplets – blue/orange, cytoplasm - green, mitochondria - magenta, cell border - light grey and area out of cell - dark grey.

Detailed inspection of Figure 4 provides valuable information related to the number of lipid droplets and their chemical compositions. To quantify the number of lipid droplets in normal astrocytes and high-grade glioblastoma, we counted the number of lipid droplets per cell in the microscopy images of Oil Red O-stained cells and Raman images of fixed regions. U-87 MG cell line contains the average number of lipid droplets of 67 per cell and NHA 29 LDs/cell, respectively.

bioRxiv preprint doi: https://doi.org/10.1101/2020.05.05.078410; this version posted May 5, 2020. The copyright holder for this preprint (which was not certified by peer review) is the author/funder. All rights reserved. No reuse allowed without permission.

First, Figures 4 (A, B, L) clearly show that cancer cells of U-87 MG high-grade brain glioblastoma contain significantly more lipid droplets than NHA normal astrocyte cells. An increased number of lipid droplets was correlated with increased aggressiveness of the brain cancer. To quantify the number of lipid droplets in normal astrocytes and high-grade glioblastoma, we counted the number of lipid droplets per cell in the microscopy images of Oil Red O-stained cells and Raman images of fixed regions. The number of lipid droplets in individual cells was also scored quantitatively by cluster analysis by measuring the area of separated clusters corresponding to lipid droplets, mitochondria and nucleus. The increased number of cytoplasmic lipid droplets in human brain cells must be closely related to the increased rate of de novo lipid synthesis in cancer cells; however, the detailed mechanisms are still unknown.

Second, based on a detailed analysis of the chemical composition of lipid droplets of NHA normal astrocytes and U-87 MG high-grade glioblastoma cells by combining cluster analysis and Raman imaging, we found two types of lipid droplet Raman profiles, which are presented in Figures 4(C) and 4(H). The composition of lipid droplets in normal astrocytes NHA contains almost exclusively Profile II, which represents lipid droplets filled with retinoids and a small amount of lipid droplets represented by Profile I representing lipid droplets filled with triglycerides (TAG). In contrast, U-87 MG high-grade glioblastoma is dominated exclusively by lipid droplets filled with triglycerides (TAG) (Profile I). Indeed, the comparison between Raman images of the distribution of retoinoid -rich lipid droplets in Figure 4(G) with TAG-rich lipid droplets in Figure 4(F) provides clear evidence that most lipid droplets in normal astrocytes accumulate retinoids rather than TAG. By contrast, lipid droplets in glioblastoma almost exclusively accumulate TAG compounds (Figures 4(J) and 4(H)). Using various wavelengths of excitation in Raman spectroscopy, the major components in lipid droplets of cells can be selectively enhanced by such resonance-enhancement effect and can be clearly visualized by Raman imaging.

Figure 5 shows the absorption spectra of retinoids, TAG (glyceryl tripalmitate) and retinol binding protein (RBP). Most TAGs and RBP exhibit negligible absorption in comparison to retinoids.

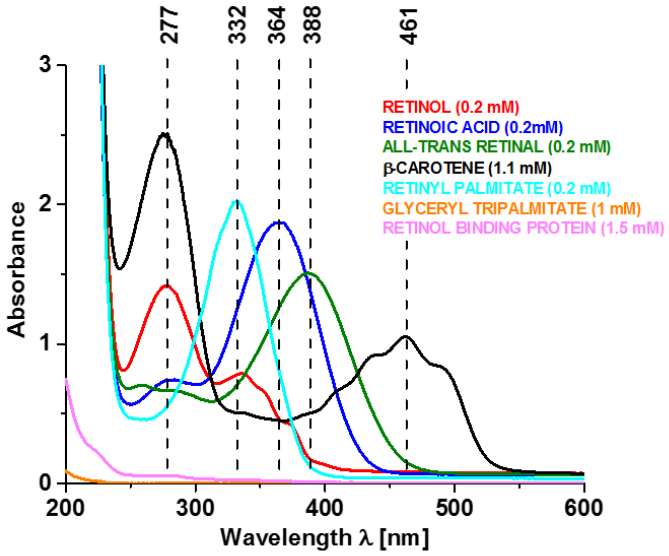

Figure 5. Absorption spectra of retinoids, TAG (glyceryl tripalmitate) and retinol binding protein. Retinol (c=0.2 mM in chloroform, red), retinoic acid (c=0.2 mM in chloroform, blue), all-trans retinal (c=0.2 mM in chloroform, green), β-carotene (c=1.1 mM in chloroform, black), retinyl palmitate (c=0.2 mM in chloroform, cyan), glyceryl tripalmitate (1 mM in hexane, orange) and retinol binding protein (1.5 mM, magenta), with a cuvette path length of 1 mm.

To address questions regarding selectively enhanced effects on lipid droplet alterations upon laser excitation, we examined the resonance and non-resonance effects in model systems of TAGs, RBP and retinoids. The results are presented in Figure 6. Figure 6(A) and 6(B), show the Raman spectra of retinyl

bioRxiv preprint doi: https://doi.org/10.1101/2020.05.05.078410; this version posted May 5, 2020. The copyright holder for this preprint (which was not certified by peer review) is the author/funder. All rights reserved. No reuse allowed without permission.

palmitate (RP) in oleic acid (OA) at 532 nm and 355 nm, respectively, at different polarization configurations.

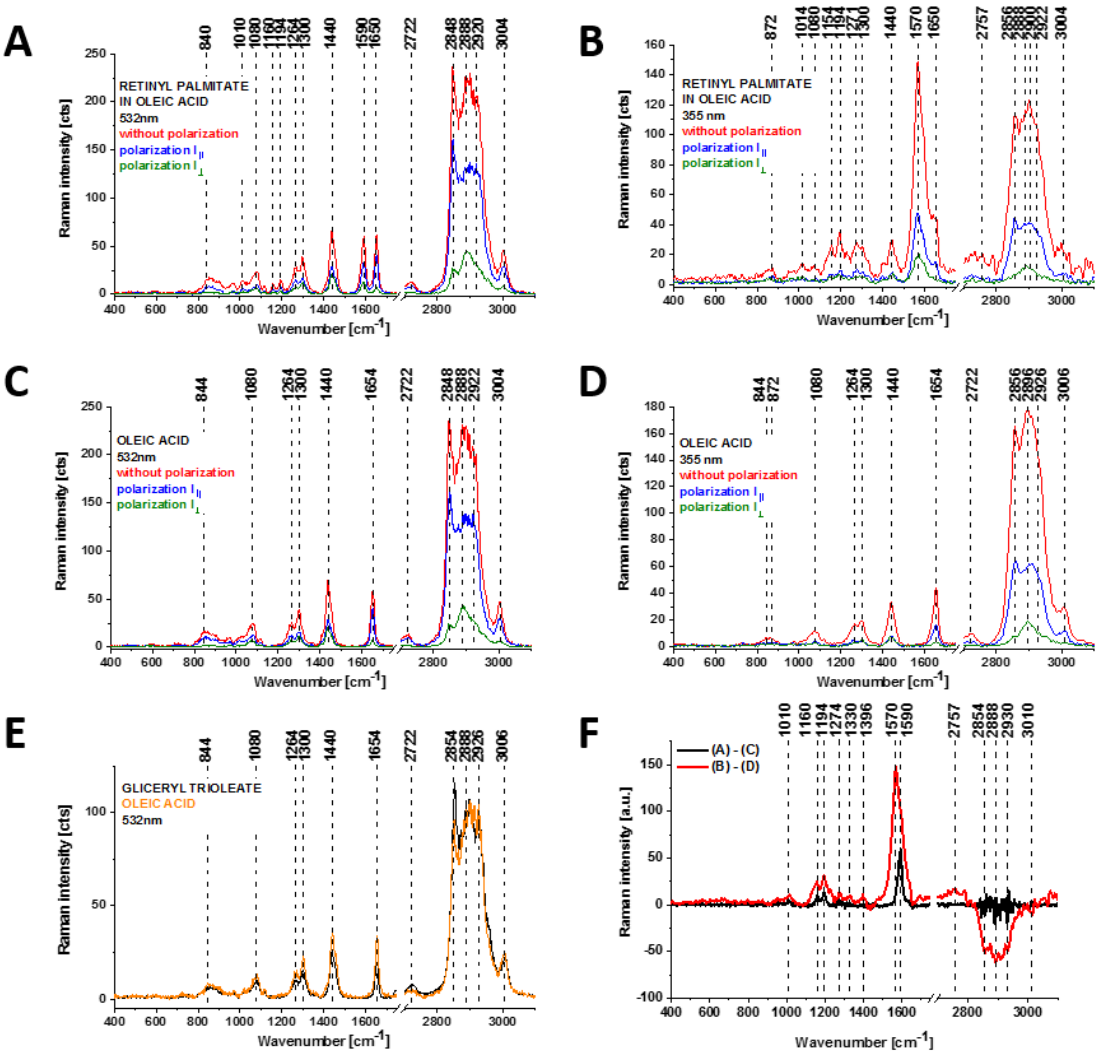

Figure 6. Raman spectra of retinyl palmitate (RP) in oleic acid (OA) (A,B) and oleic acid (C,D) under different polarization configurations (non-polarized (red), parallel polarization III (blue), perpendicular polarization I⊥ (green) at 532 nm (A,C) and 355 nm (B,D) and Raman spectra of TAG (glyceryl trioleate) and oleic acid (E) at 532 nm. (F) Difference spectra of (A)-(C) and (B)-D).

The results presented in Figure 6 clearly demonstrate that TAG compounds (OA (Figure 6 (C,D), glyceryl trioleate (E)) show no Raman resonance enhancement in contrast to retinyl palmitate (Figure 6 (A,B)), with the characteristic band of RP at 1590 cm^{-1} for 532 nm. This band disappears at 355 nm due to photochemical reactions that occur upon 355 nm excitation, as presented in Figures 7 and a new band at 1570 cm^{-1} corresponding to all-trans retinol appears. The band at 1570 cm^{-1} is significantly enhanced by the resonance Raman effect due to the absorption of retinol at 355 nm presented in Figure 5.

bioRxiv preprint doi: https://doi.org/10.1101/2020.05.05.078410; this version posted May 5, 2020. The copyright holder for this preprint (which was not certified by peer review) is the author/funder. All rights reserved. No reuse allowed without permission.

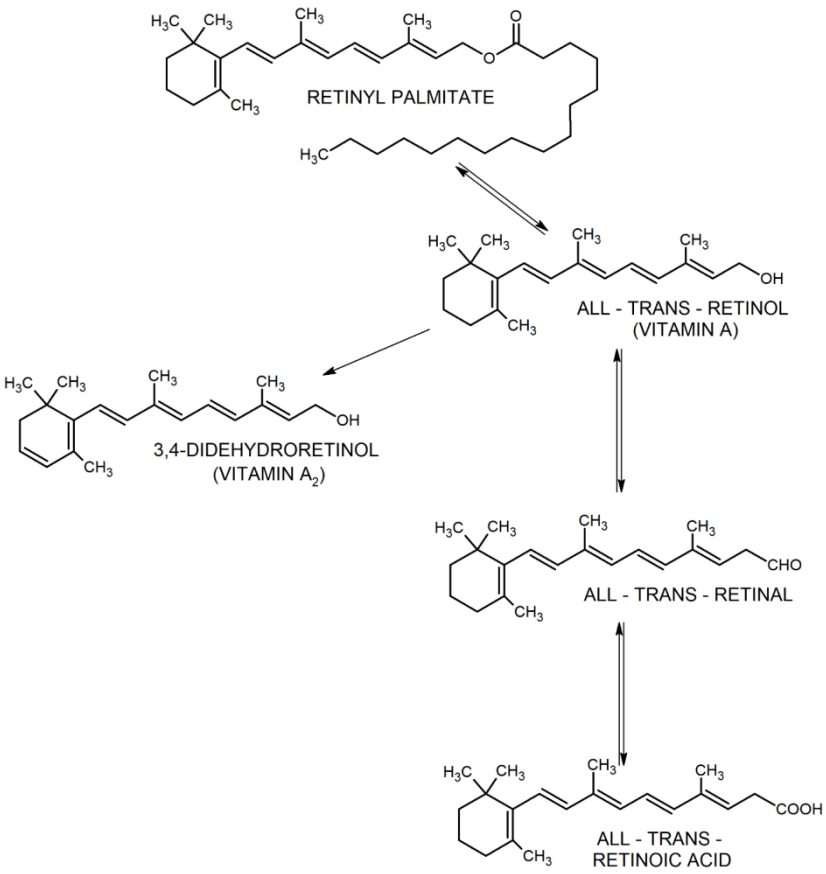

Figure 7. Photochemical reactions of retinoids upon 355 nm excitation.

The results presented herein for model systems demonstrate that Raman microscopy and imaging are excellent tools to monitor the role of retinoids in single cells and tissues.

Figure 8 shows the Raman spectra at 532 nm of retinoids: retinyl palmitate, all-trans-retinol, all-trans-retinal, all-trans retinoic acid with the characteristic bands at 1570 cm^{-1} (retinoic acid, retinal) and 1590 cm^{-1} (retinol, retinyl palmitate). The high frequency vibrations in the range 2800-3100 cm^{-1} show three types of Raman band profiles: profile A - for retinol, retinal, RBP-1; profile B - retinoic acid; profile C- retinyl palmitate. Detailed analysis of biochemical profiles showed that Profile II in Figure 4 and profile A in Figure 8 are identical suggesting that the lipid droplets in normal astrocytes NHA are filled with retinol and/or retinyl esters.

bioRxiv preprint doi: https://doi.org/10.1101/2020.05.05.078410; this version posted May 5, 2020. The copyright holder for this preprint (which was not certified by peer review) is the author/funder. All rights reserved. No reuse allowed without permission.

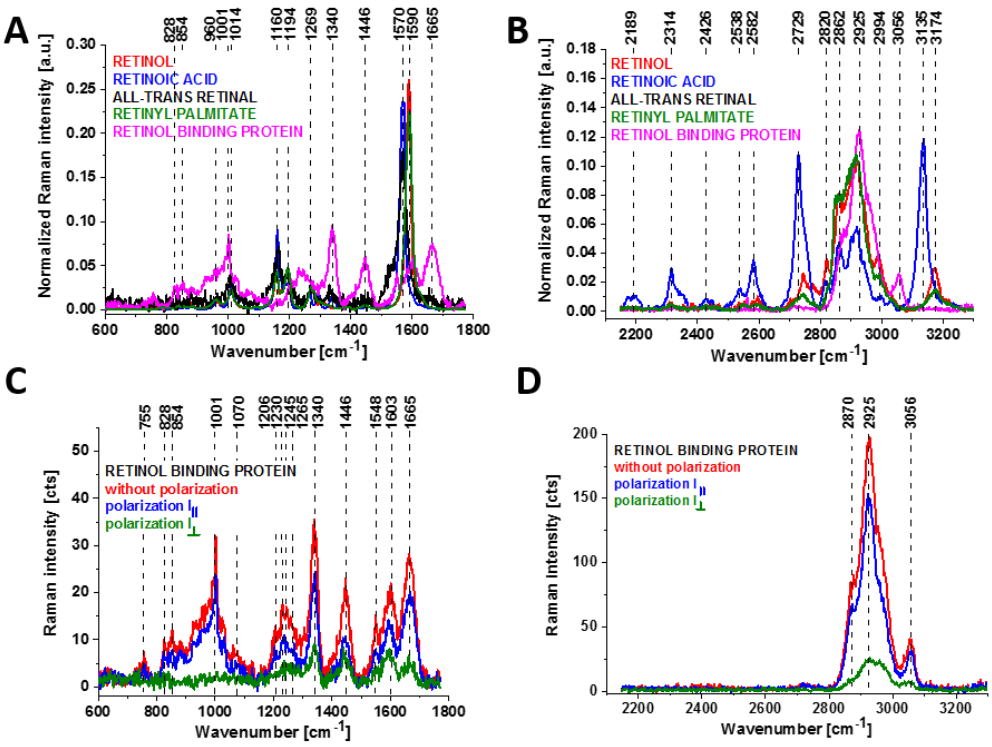

Figure 8. Raman spectra of the retinoids involved in photochemical reactions (A,B) and non-polarized and polarized Raman spectra of retinol binding protein RBP-1 (C,D) (non-polarized (red), parallel polarization (blue), perpendicular polarization (green)). Raman spectra were recorded at 532 nm wavelength excitation.

Figure 8 shows the Raman spectra of retinol-binding protein (RBP-1) with the characteristic vibrations of amide I (1665 cm^{-1}), amide II (1603 cm^{-1}, 1548 cm^{-1}), the tyrosine doublet at 828 cm^{-1} and 854 cm^{-1} representing the tyrosine residue of RBP-1 corresponding to a Fermi-resonance between the first overtone of the aromatic out-of-plane ring bending mode and the breathing fundamental aromatic ring[50,51], and the band at 1265 cm^{-1} corresponding to amide III and red-shifted to the 1230 cm^{-1} band of amide III upon phosphorylation.[51,52] Vibrations of the PO_4^- phosphate group of phosphorylated tyrosine were observed at 1070 cm^{-1} and corresponded to the O-P-O symmetric stretching mode.[51–55]

We found that retinoids in Figure 6 are sensitive to the resonance Raman enhancement. Now, we want to find and examine the resonance and non-resonance effects of retinoids in the biochemical Raman maps of cellular organelles in cell cultures of normal astrocytes (NHA) and glioblastoma (U-87 MG) as a function of the laser wavelength excitation to examine the Raman signal under resonance and non-resonance conditions.

Figure 9 shows the Raman spectra and images of U-87 MG glioblastoma and NHA normal astrocytes at 355, 532 and 785nm.

bioRxiv preprint doi: https://doi.org/10.1101/2020.05.05.078410; this version posted May 5, 2020. The copyright holder for this preprint (which was not certified by peer review) is the author/funder. All rights reserved. No reuse allowed without permission.

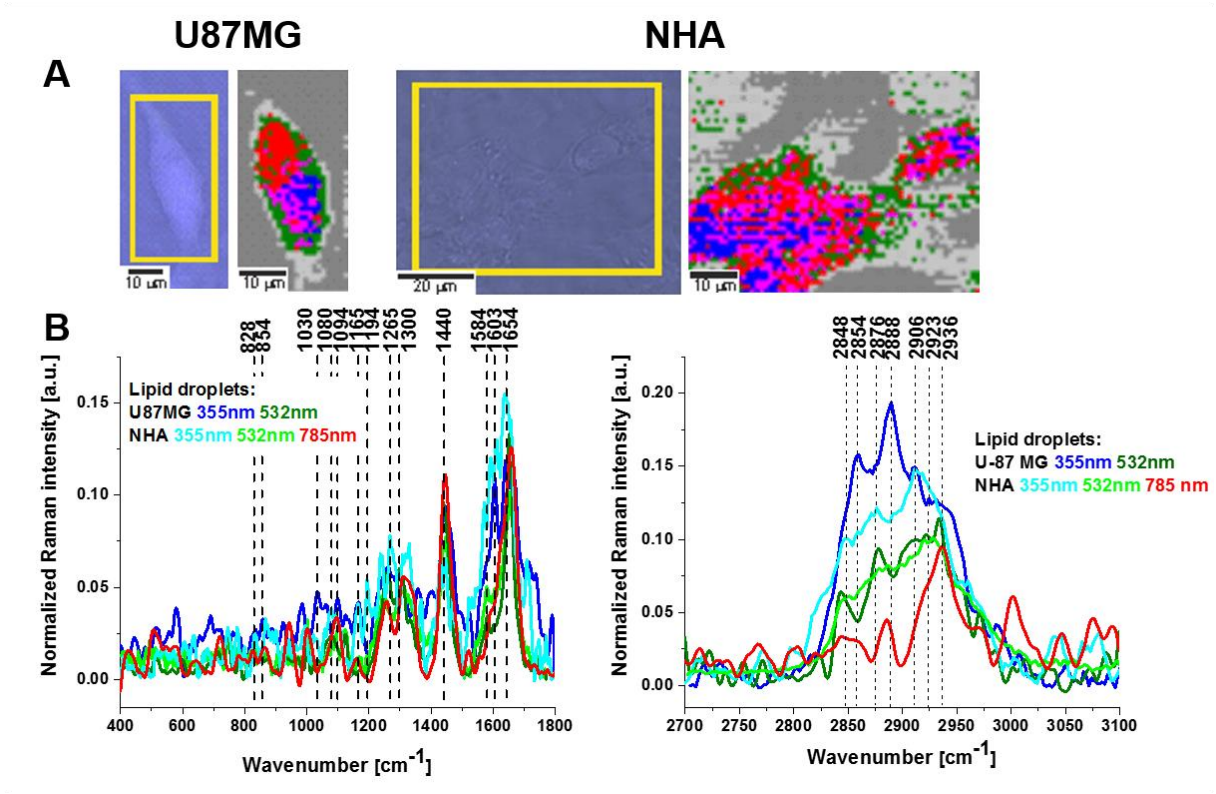

Figure 9. Comparison of normal astrocytes (NHA) and high grade glioblastoma (U-87 MG). Microscopy images, Raman images (excitation at 355 nm) (A) and Raman spectra of lipid droplets at 355, 532 and 785 nm (B).

The red, blue and pink areas in Raman cluster images in Figure 9(A) represent nuclei, lipid droplets and mitochondria, respectively. Lipid droplets are typically localized in strings adjacent to the nucleus (as seen in Figure 3) or randomly distributed in the cytosol, the mitochondria are clustered around the lipids. It has been suggested that lipid droplets are not only an energy storage source for mitochondria, but also mitochondria play an important role in helping to build the lipid droplets.[56]

A detailed inspection of Figure 9(B) reveals notable differences in the Raman vibrations of lipid droplets at different wavelengths. Figure 9(B) shows that the average Raman profile of lipid droplets is significantly different at 355 nm, 532 nm and 780 nm corresponding to resonance and non-resonance conditions both for cancer and normal cells. Figure 9 shows that the Raman intensity of the band at 1584 cm^{-1} increased at 355 nm and 532 nm and diminished at 785 nm, indicating that the chromophore attached to the protein is absorbed in the range from 355-532 nm.

The results are consistent with those obtained for the cancer tissues presented in Figure 2, indicating that both lipid droplets and cancer brain tissue contain compounds that are enhanced at 355 nm corresponding to Raman resonance conditions.

The results presented thus far provide strong evidence that lipid droplets accumulate retinoids and TAG lipids. We next detailed the differences in the chemical composition of lipid droplets, mitochondria and the nucleus in normal astrocytes and high-grade malignant human brain cells (glioblastoma). We compared the alterations in the chemical composition of lipid droplets, nuclei and mitochondria of normal astrocytes NHA and high-grade glioblastoma (U-87 MG).

Figure 10 shows a comparison of the average Raman spectra obtained from the cluster analysis of lipid droplets, mitochondria and nuclei of normal human astrocytes (NHA) and high-grade glioblastoma (U-87 MG) at 532 nm excitation.

bioRxiv preprint doi: https://doi.org/10.1101/2020.05.05.078410; this version posted May 5, 2020. The copyright holder for this preprint (which was not certified by peer review) is the author/funder. All rights reserved. No reuse allowed without permission.

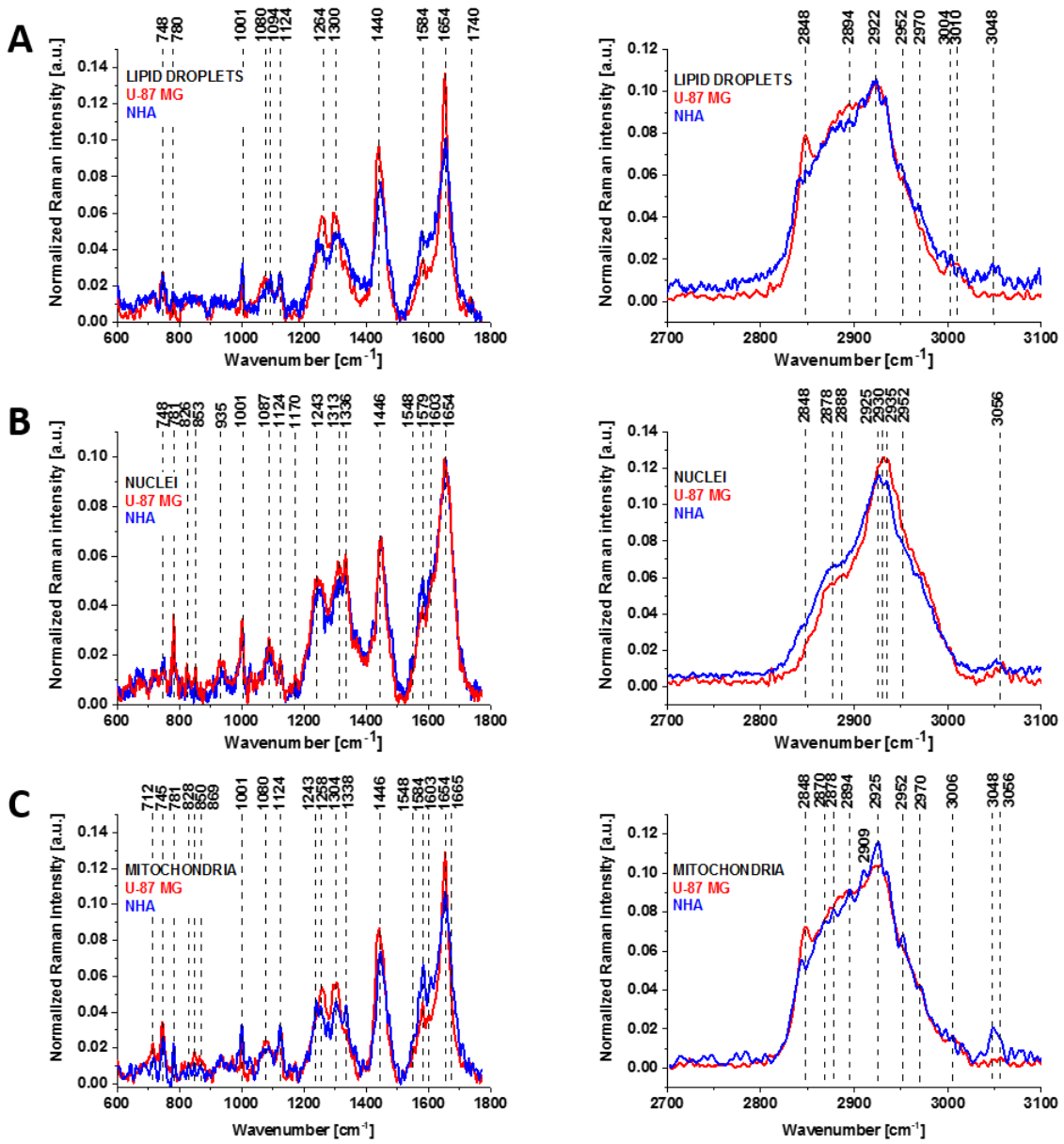

Figure 10. The average Raman spectra obtained at 532 nm wavelength laser excitation from the cluster analysis of lipid droplets (A), nuclei (B) and mitochondria (C) of normal human astrocytes (NHA, blue) and high-grade glioblastoma (U-87 MG, red).

Detailed inspection of Figure 10 revealed that clear differences between NHA normal human astrocytes and U-87 MG high-grade glioblastoma in all studied organelles occurred in the same regions of vibrations that were sensitive to Raman resonance enhancement due to the retinoid absorption at 350 nm and observed at 1584 cm^{-1} and 1654 cm^{-1} and in the high frequency region at 2848 cm^{-1} (corresponding to TAG lipids) and 2923 cm^{-1} corresponding to both TAG, retinoids, and retinol binding proteins. The origin of the protein band at 1584 cm^{-1} is not clear. The bands at 1584 cm^{-1} and 1655 cm^{-1} cover the spectral region corresponding to the amide II and amide I vibrations of proteins with Raman signatures characteristic of tyrosine residues[57], cytochrome family and retinol binding proteins. Retinol binding proteins belong to lipocalin family with the concentration of RBP in serum around 40 to 50 μg/ml, which indicates that they are undetectable at non-resonance conditions at 532 nm. They would be detectable at 1584 cm^{-1} only in the complex RBP-retinol with eight antiparallel β sheets in the centre which binds retinol[58] due to retinol Raman enhancement. In contrast, the cytochrome family

bioRxiv preprint doi: https://doi.org/10.1101/2020.05.05.078410; this version posted May 5, 2020. The copyright holder for this preprint (which was not certified by peer review) is the author/funder. All rights reserved. No reuse allowed without permission.

with Q-band absorption at 500-550 nm is in resonance with 532 nm excitation and the band 1584 cm^{-1} may correspond to cytochrome c.

Figure 10 shows that the Raman signal intensity of the band at 1584 cm^{-1} in lipid droplets is significantly enhanced for normal astrocyte (NHA) compared with high-grade glioblastoma (U-87 MG). The 1584/1654 Raman intensity ratio of the bands at 1584 cm^{-1} and 1654 cm^{-1} was 0.59 for lipid droplets in NHA and 0.27 for lipid droplets in U-87 MG. Moreover, the 2848/2923 Raman intensity ratio of the bands at 2848 cm^{-1} and 2923 cm^{-1} was 0.59 for NHA and 0.72 for U-87 MG, indicating a lower concentration of TAG lipids (and a higher concentration of retinyl esters) in NHA normal cells than U-87 MG cancer cells. The 1584/1654 Raman intensity ratios for mitochondria were also significantly higher (0.88) for NHA than U-87 MG (0.75), indicating a higher concentration of retinol binding proteins in the mitochondria of normal NHA cells. The 2848/2923 ratio for mitochondria was 0.74 in NHA and 0.82 in U-87 MG, indicating a lower concentration of TAG lipids in NHA normal cells than U-87 MG cancer cells. The 1584/1654 Raman intensity ratio for nuclei was also significantly higher (0.83) for NHA than U-87 MG (0.770).

The results presented in Figure 10 and Table 1 reveal the lower expression of proteins proteins represented by the band at 1584 cm^{-1} in human brain cancer. Second, the Raman signal intensity of the band at 2848 cm^{-1} in lipid droplets was significantly higher for high-grade cancer of glioblastoma (U-87 MG) than for normal astrocytes (NHA), indicating a higher concentration of TAG in lipid droplets. The higher concentration of TAG was related to the increased amount of cytoplasmic lipid droplets in human brain cells in comparison to normal astrocytes. By contrast, the intensity of the band at 2848 cm^{-1} in the nucleus was higher in NHA than in U-87 MG.

Table 1. Comparison of the Raman intensity ratio of lipid droplets, mitochondria and nuclei for NHA and U-87 MG cell lines, presented as the mean±SD.

	Lipid droplets		**Mitochondria**		**Nuclei**
	I (1584 cm^{-1})/ I (1654 cm^{-1})	**I (2848 cm^{-1})/ I (2923 cm^{-1})**	**I (1584 cm^{-1})/ I (1654 cm^{-1})**	**I (2848 cm^{-1})/ I (2923 cm^{-1})**	**I (1584 cm^{-1})/ I (1654 cm^{-1})**
NHA	0.59±0.11	0.59±0.09	0.88±0.18	0.74±0.03	0.83±0.17
U-87 MG	0.27±0.06	0.72±0.07	0.75±0.06	0.82±0.05	0.77±0.08

To clarify the origin of the band at 1584 cm^{-1}, which is crucial for understanding the role of retinoids we incubated the glioblastoma cells (U-87 MG) with retinoic acid (RA) and with retinol (ROL). Figure 11 shows the Raman spectra of nucleus, lipid droplets and mitochondria in the U-87 MG cells incubated with RA and ROL. As one can see from Figure 11 retinoic acid (spectrum marked on red) exerts a spectacular effect on the Raman spectra of glioblastoma cells, particularly on the band at 1584 cm^{-1} when compared with the control cells without RA (black spectrum). The similar effect is observed for Raman spectra of the U-87 MG cells incubated with ROL, but there are some marked differences. First, the Raman signal intensity ratio of the bands at 1590 and 1655 cm^{-1} 1590/1655 for retinol effect is significantly smaller than the ratio of 1584/1655 for retinoic acid in glioblastoma cells. Second, the maximum of the Raman band at 1584 cm^{-1} in RA is shifted to 1590 cm^{-1} corresponding to the vibrations of retinol and retinyl palmitate (see Figure 8A) indicating that the lipid droplets and mitochondria are filled with retinol.

bioRxiv preprint doi: https://doi.org/10.1101/2020.05.05.078410; this version posted May 5, 2020. The copyright holder for this preprint (which was not certified by peer review) is the author/funder. All rights reserved. No reuse allowed without permission.

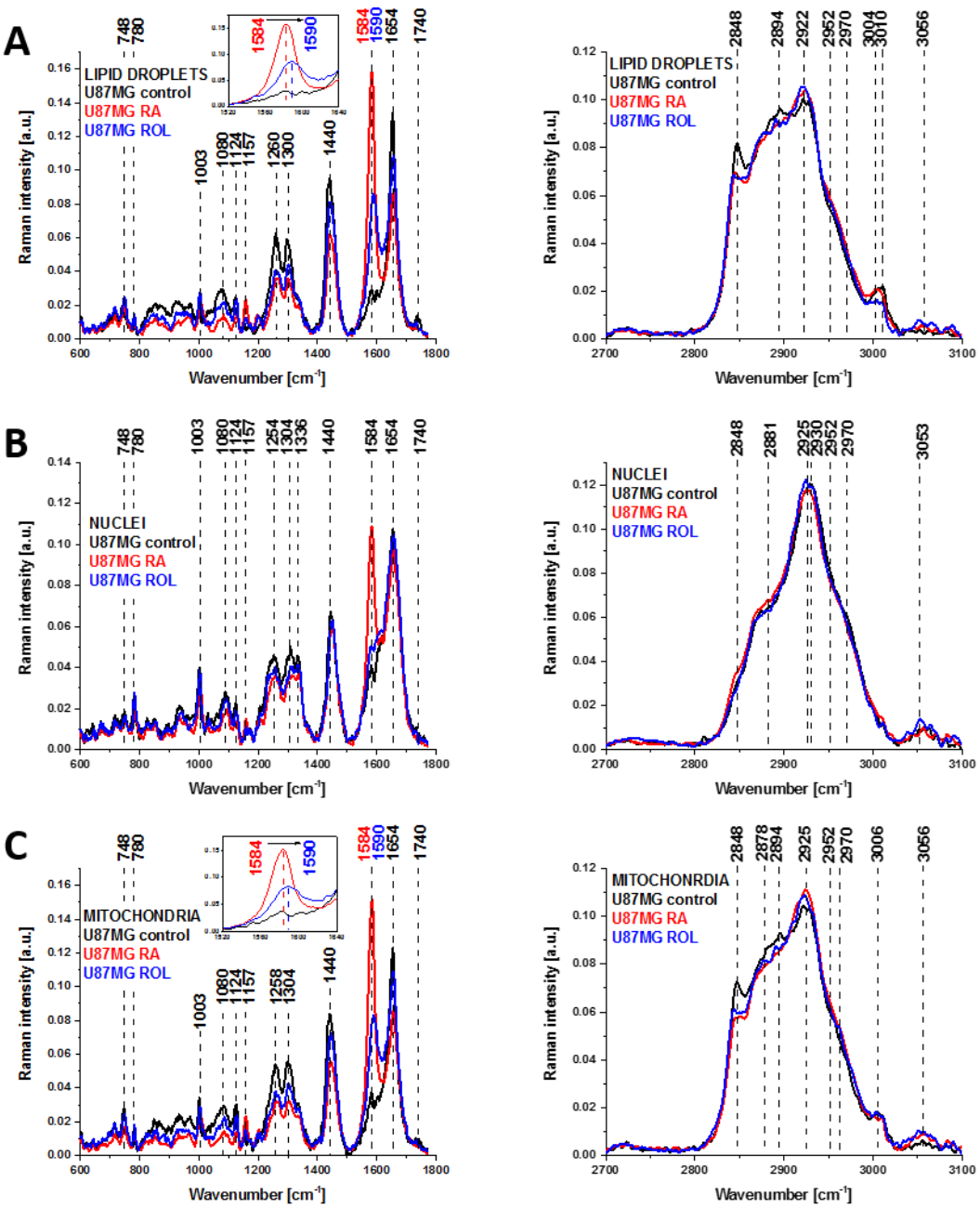

Figure 11. The average Raman spectra obtained at 532 nm wavelength laser excitation from the cluster analysis of lipid droplets (A), nuclei (B) and mitochondria (C) of high-grade glioblastoma (U-87 MG) incubated with retinoic acid (RA, red) and retinol (ROL, blue) (concentration of 50 μM, incubation time of 24 hours).

Based on detailed Raman analysis of lipid droplets, mitochondria and nucleus, we identified a protein that exhibits an enhanced Raman resonance signal for retinoids, which was found mainly in lipid droplets and mitochondria. The protein has β sheets structure and vibrational signatures characteristic of the cytochrome c and phosphorylation activity of tyrosine residues.[57] The protein is coupled with retinoids, particularly retinoic acid and retinol. We suspect that the 1584 cm^{-1} band originates from a small protein involved as an intermediate in the electron transport chain in mitochondria, most probably in the cytochrome c oxidase, where the electron transport is blocked due to cancer development. This unidentified protein is more likely to be a cytochrome c. We are making intensive efforts to identify unambiguously this mysterious unknown protein, which must be playing a

bioRxiv preprint doi: https://doi.org/10.1101/2020.05.05.078410; this version posted May 5, 2020. The copyright holder for this preprint (which was not certified by peer review) is the author/funder. All rights reserved. No reuse allowed without permission.

key role in the respiratory activity in mitochondria and hence is essential for the life of a normal and tumor cells.

Our results are consistent with data obtained for retinol binding protein (RBP-1)[1] showing that wild-type RBP-1 (also known as CRBP-1) has lower expression in cancers. The results presented in Figure 10 and Table 1 reveal the lower expression of proteins represented by the band at 1584 cm^{-1} in human brain cancer. Our results are consistent with those reported recently.[1,25,31] where lower expression of cellular retinol-binding protein (CRBP-1) has been observed in breast and other human cancers, but its significance is not well understood.[1,25,31] The results fully support the importance of retinoids and retinol binding proteins in brain carcinogenesis. Research has demonstrated that overexpression of CRBP-1 increases the ability of RBP-retinol complex to phosphorylate STRA6 and, later, JAK2 and STAT5.[2]

Discussion

The present results analysed in the context of recent studies[1,11,56] suggest that the processes that occur in lipid droplets play an important role in the molecular mechanisms of brain carcinogenesis. The localization of retinol binding protein 1 in lipid droplets associated with retinol accumulation suggests that lipid droplets are involved in a chain of events starting from the entry of retinol into the interior of the cell to the final stage of induction of target gene expression in the nucleus. Although the role of vitamin A in these processes remains poorly understood, many studies together with the results presented in this paper will shed light on its role in carcinogenesis.

Our results show the interplay between retinol, retinol binding proteins, cytochrome c and enhanced de novo lipid synthesis.

Considering the results presented in this paper, growing evidence suggests a far more fundamental role for retinol than previously reported. Our results suggest that retinol is essential both for signal transduction and metabolic reprogramming in cancer cells, and these processes depend on each other. To illuminate the role of retinoids we hypothesize that vitamin A plays a key role in switching the metabolic path from oxidative phosphorylation in the mitochondrion to glycolytic fermentation in the cytosol and propose the following sequence of events to explain the interplay between the signaling and metabolic pathways.

1) Retinoids may play a key role in controlling energy metabolism in the cell during the process of triggering ATP synthase via the electrostatic gradient in the inner mitochondrial membrane. The mechanism of altered energy metabolism that replaces the more efficient oxidative phosphorylation to yield adenosine triphosphate (ATP) with the less efficient glycolysis represents a pivotal problem that must be solved to achieve progress in cancer research. We hypothesize that vitamin A plays a key role in switching the metabolic path from oxidative phosphorylation in the mitochondrion to glycolytic fermentation in the cytosol.

2) Our results suggest that switching the metabolic path from oxidative phosphorylation in the mitochondrion to glycolytic fermentation in the cytosol depends on a deficiency of vitamin A and/or low level of the retinol binding proteins (possibly acceptor CRBP-1 and/or cytochrome c), resulting in reduced production of ATP in mitochondria in cancer cells. The disrupted ATP synthase functions originates from the lower electrostatic gradient in the mitochondrial cell membrane.

3) Retinoids (retinoic acid, retinol) generate a higher gradient in the mitochondrial cell membrane. A few explanations are possible, one of which suggests that retinol in mitochondria is an essential cofactor of protein kinase C delta (PKC delta), without which PKC delta cannot be activated in mitochondria. According to ref.[33], the PKC delta/retinol complex triggers the pyruvate dehydrogenase complex for enhanced flux of pyruvate into the Krebs cycle. PKC kinase belongs a family of serine and threonine-specific protein kinases that can be activated by calcium and the second messenger diacylglycerol.[33]

4) Another explanation for the higher electrochemical gradient generated by retinol may be related simply to the additional source of electrons provided by retinol/retinoic acid. At normal physiological

bioRxiv preprint doi: https://doi.org/10.1101/2020.05.05.078410; this version posted May 5, 2020. The copyright holder for this preprint (which was not certified by peer review) is the author/funder. All rights reserved. No reuse allowed without permission.

conditions electrons are generated in the electron transport chain organized in terms of electronegativity where the reduction of NAD^+ to NADH (and FAD to FADH2) and oxidation play important roles.

5) When the Krebs cycle is deactivated by retinol in cancer cells, acetyl CoA cannot be metabolized by the Krebs cycle, the reduction of NAD^+ to NADH (and FAD to FADH2) is blocked and high-energy electrons cannot be produced from NADH (and FADH2). The lack of electron transport along the electron-transport chain in the inner membrane of the mitochondrion to oxygen (O_2) prevents the generation of a proton gradient across the inner membrane, which is used to trigger the production of ATP by ATP synthase. When the Krebs cycle is deactivated by retinol, the cell switches to glycolysis in the cytosol.

6) When the Krebs cycle is deactivated by retinol, cancer cells, which need ATP for survival, must switch to glycolytic fermentation in the cytosol, which is less favorable in terms of energy storage but is much faster. Inside mitochondria there are enzymes that metabolize pyruvate and fatty acids to produce acetyl CoA, which can be used for enhanced synthesis of fatty acids that are stored in lipid droplets when the flux of pyruvate into the Krebs cycle is reduced. The role of de novo lipid synthesis increases in cancer cells.

This model explains the increased production of lipid droplets that we observed in cancer cells of U-87 MG glioblastoma when compared with normal astrocytes. The model explains also the differences in chemical composition of normal astrocytes and in the cancer cells of glioblastoma. Under normal physiological conditions, lipid droplets serve as a source of retinyl ester storage, resulting in a reduced concentration of retinol in the cytosol and a higher concentration unbound to retinol CRBP-1 proteins required for normal functioning of retinol transport via membrane STRA6. In cancer cells where oxidative phosphorylation in mitochondria is replaced by glycolysis in the cytosol, CoA is used for enhanced de novo fatty acid synthesis and storage of TAG in lipid droplets during a reduced flux of pyruvate into the Krebs cycle.

Precise information regarding the role of retinoids and retinol binding proteins is relevant both for basic cancer research and clinical applications. Understanding the metabolism of retinoids in normal and brain cancer cells is still very limited because there are no experimental methods available to track retinoids in vivo in living cells.

This paper addresses the role of retinol and cellular retinoid-binding proteins in normal and cancer cells, especially the selective cellular uptake, intracellular transport, and metabolism of retinoids in normal and brain cancer cells.

We report a method for tracking the spatial distribution of retinoids and retinoid binding proteins in cells using label-free hyperspectral Raman microscopy and multivariate chemometric analysis in normal human astrocytes and high-grade brain cancer cells of glioblastoma. This method allows the chemical composition mapping of lipid droplets, mitochondria, and nuclei in single cells. It also allows the tracking of intracellular retinoid metabolism and the discrimination of lipid droplets from mitochondria and nuclei in normal and cancer cells.

Here we report the spectral identification of retinoids accumulation in specific cell organelles by label-free hyperspectral Raman microscopy and imaging. Raman polarization measurements have revealed the occurrence of conformational changes that affect discrete regions of the protein molecule associated with retinol binding.

We discovered previously unknown two types of lipid droplets with distinct chemical compositions, biological functions and vibrational properties. The composition of the lipid droplets in cancer cells are dominated by triglycerides (TAG), both for medulloblastoma and glioblastoma tissues and glioblastoma cells (U-87 MG). The lipid droplets in normal astrocytes NHA are dominated by retinyl esters as well as their retinoid derivatives.

As the composition of the lipid droplets in normal, low-grade and high-grade malignant human brain cells showed remarkable differences we suggest that this is associated with different functions regulated by the proportion between TAGs and retinyl esters. The two types of lipid droplets are related to different functions - energy storage and signaling. Their expression and biochemical composition depends on cancer aggressiveness. The first group is dominantly filled with TAGs and is involved in

bioRxiv preprint doi: https://doi.org/10.1101/2020.05.05.078410; this version posted May 5, 2020. The copyright holder for this preprint (which was not certified by peer review) is the author/funder. All rights reserved. No reuse allowed without permission.

energy storage. The second group is filled mainly with retinyl esters /retinol and is involved in signaling, especially JAK2/STAT6 pathway signaling. An understanding of JAK2/STRA6 signaling is clinically relevant in cancer, but a detailed potential role for STRA6 awaits further investigation.

We found a higher concentration of the retinol binding proteins and a lower concentration of TAG lipids in NHA normal cells than in aggressive tumor cells of U-87 MG. The Raman intensity ratio 2848/2923 of the TAG bands at 2848 and 2923 cm^{-1} for mitochondria was 0.74 in NHA and 0.82 in U-87 MG, indicating a lower concentration of TAG lipids in NHA normal cells than in U-87 MG cancer cells.

To summarize, the present results fully support the importance of retinoids and retinol binding proteins in brain carcinogenesis. The proteins have β sheets structure and vibrational signatures characteristic of the cytochrome c and phosphorylation activity of tyrosine residues.[57] The protein is coupled with retinoids, particularly retinoic acid and retinol.

Materials and Methods

Reference chemicals

All trans-retinal (no. R2500), 13-cis–retinol (no. R0271), retinol palmitate (no. 46959-U), retinol binding protein from human urine (no. R9388), retinol (no. R7632), retinoic acid (np. R2625), an all trans-retinal (no. R2500) were purchased from Sigma Aldrich and all-trans-retinyl oleate (no. sc-476306) from Santa Cruz Biotechnology.

Cell culture and preparation for Raman/fluorescence spectroscopy

A normal human astrocyte (NHA) cell line (CC-2565; Lonza) and human glioblastoma (U-87 MG) cell line (HTB-14; ATCC) were used. NHA cells were grown in AGM BulletKit (Lonza CC-3186). U-87 MG cells were grown in EMEM with 2 mM glutamine, 1% non-essential amino acids (NEAA), 1 mM sodium pyruvate (NaP) and 10% foetal bovine serum (FBS). All cell lines were maintained at 37°C in a humidified atmosphere containing 5% CO_2. Cells for Raman spectroscopy analysis were seeded on a 25-mm round CaF_2 window placed in a 35-mm Petri dish at a density of $5x10^4$ cells per Petri dish.

Before the Raman measurements, the cells were washed with phosphate-buffered saline (PBS) to remove any unattached cells, fixed in neutral buffered 10% formalin and washed with PBS. After the Raman imaging measurements, the cells were exposed to Hoechst 33342 (25 μL at 1 μg/mL per mL of PBS) and Oil Red O (10 μL of 0.5 mM Oil Red dissolved in 60% isopropanol/dH2O per each mL of PBS) by incubation for 15 min. The cells were then washed with PBS, followed by the addition of fresh PBS for fluorescence imaging on an Alpha 300RSA WITec microscope. Mitochondria were stained by Mitotracker Red CMXROS (M7512, at a final concentration of 100 nM Mitotracker Red CMXROS for 15 mins).

Tissue preparation for Raman spectroscopy

Raman spectra and images were analysed from patients with brain tumours. All of the procedures for human tissues were conducted under a protocol approved by the institutional Bioethical Committee at the Medical University of Lodz (RNN/323/17/KE/17/10/2017). All of the brain experiments were performed in compliance with the relevant laws and guidelines of the Bioethical Committee at the Polish Mother's Memorial Hospital Research Institute in Lodz (no. 53/216). Written informed consent was obtained from all patients, or if subjects are under 18, from a parent and/or legal guardian.

The ex-vivo samples were obtained during resection surgery from the tumour mass. All tissue specimens were frozen and stored at -80 ºC. Before the measurements, the frozen samples were cryosectioned at - 20 ºC with a microtome (Microm HM 550, Thermo Fisher, Waltham, USA) into 16 μm thick slices and placed onto calcium fluoride windows (CaF_2, 25 ×1 mm, Crystal GmbH, Berlin, Germany).

bioRxiv preprint doi: https://doi.org/10.1101/2020.05.05.078410; this version posted May 5, 2020. The copyright holder for this preprint (which was not certified by peer review) is the author/funder. All rights reserved. No reuse allowed without permission.

Raman data acquisition and analysis

Raman spectroscopy measurements were performed with a confocal Raman microscope (Alpha 300RSA, WITec, Ulm, Germany) equipped with 355, 532 and 785 nm diode lasers, a 300-mm triple grating imaging spectrometer (Acton SpectraPro SP-2300; Princeton Instruments Inc., USA), a thermoelectrically cooled CCD camera (Andor, Ireland), and a 40x water dipping objective. Raman peak positions were checked using reference sample (a silicon wafer Raman peak at 520.7 cm^{-1}). Raman maps were collected using a 0.3 s integration time (532 nm excitation, 10 mW power; 355 nm, 2 mW; 785 nm, 80 mW). More than 12000 Raman spectra were collected for each cell line with 3 replications.

The configuration employed in the measurements is presented in Figure 12.

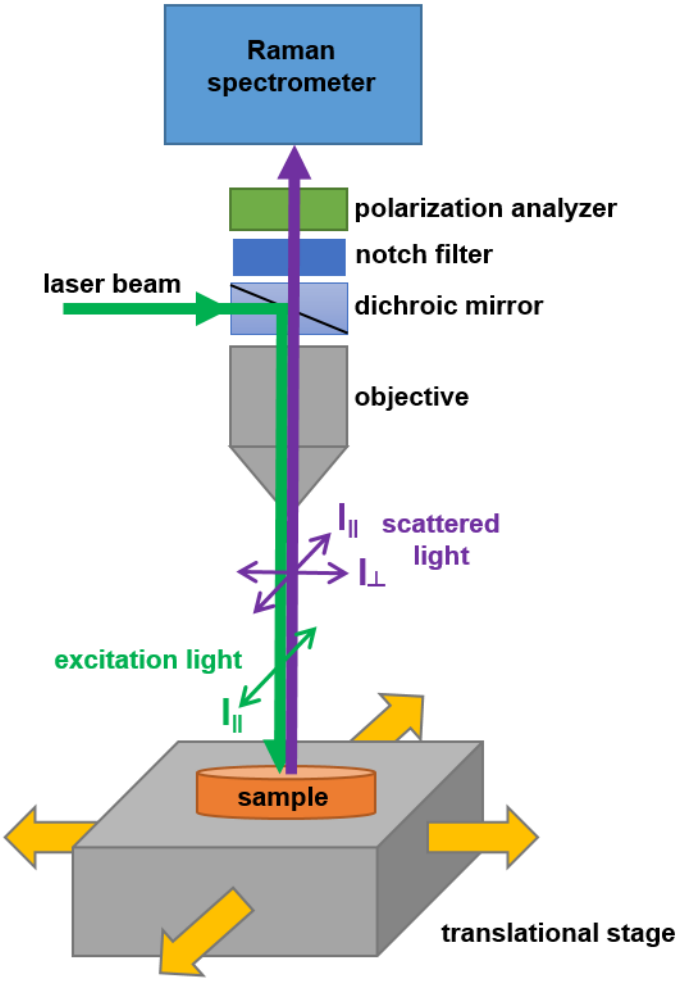

Figure 12. Configuration for polarized Raman imaging with an alpha 300 RSA+ (WITec, Ulm, Germany).

Following the removal of the polarization analyser of the scattered beam, we measured the Raman signal from all polarization directions (non-polarized Raman signal). When the polarization analyser was set at 0 º with respect to the polarization of the incident excitation beam, we measured the signal of the scattered beam with polarization parallel to the polarization of the incident beam (parallel polarization III). When the polarization analyser is set at 90 º with respect to the polarization of the incident excitation beam, we measured the signal of the scattered beam with polarization perpendicular to the polarization of the incident beam (perpendicular polarization I⊥).

Data processing was performed using Project Plus Four (WITec GmbH, Ulm, Germany) and Origin 2018 (OriginLab, Northampton, USA). All Raman spectra were cosmic ray and baseline corrected (polynomial order: 3-5) and then smoothed using a Savitzky-Golay filter (order 3, 4 pt) and vector normalized (normalized by norm). K-means clustering was performed using WITec Project Plus

bioRxiv preprint doi: https://doi.org/10.1101/2020.05.05.078410; this version posted May 5, 2020. The copyright holder for this preprint (which was not certified by peer review) is the author/funder. All rights reserved. No reuse allowed without permission.

(WITec, Ulm, Germany). The basis analysis method (BBM) was used to create the Raman images. The basis spectra that were used in BBM represented the average spectra from characteristic morphological areas in the tissue. In BBM, each recorded spectrum of the 2D spectral Raman image was compared to the basis spectrum using a least squares fit. The Raman map illustrates the weight factor at each pixel in the 2D image coded with arbitrary colours corresponding to the selected BBM spectra. The colour code of the Raman maps was based on the integrated Raman intensities in specific regions (sum option in the filter manager in the Witec Control version 4.1 software (WITec, Ulm, Germany)).

Author Contributions: Conceptualization: HA, AI, JS; Funding acquisition: HA; Investigation: AI and JS; Methodology: HA, IA and JS; Writing – original draft: HA; Writing – review & editing: HA, AI and JS. All authors reviewed and provide feedback on the manuscripts.

Funding: This research was funded by Narodowe Centrum Nauki (Poland), grant number UMO-015/19/B/ST4/01878.

Conflicts of Interest: The authors declare no conflict of interest. The funders had no role in the design of the study; in the collection, analyses, or interpretation of data; in the writing of the manuscript, or in the decision to publish the results.

Ethics approval and consent to participate: All of the procedures for human breast and small intestine tissues were conducted under a protocol approved by the institutional Bioethical Committee at the Medical University of Lodz (RNN/323/17/KE/17/10/2017). All of the brain experiments were performed in compliance with the relevant laws and guidelines of the Bioethical Committee at the Polish Mother's Memorial Hospital Research Institute in Lodz (53/216). Written informed consent was obtained from all patients, or if subjects are under 18, from a parent and/or legal guardian.

References

1. Farias EF, Ong DE, Ghyselinck NB, Nakajo S, Kuppumbatti YS, Mira y Lopez R. Cellular retinol-binding protein I, a regulator of breast epithelial retinoic acid receptor activity, cell differentiation, and tumorigenicity. J Natl Cancer Inst. 2005;97: 21–29. doi:10.1093/jnci/dji004

2. Berry DC, O'Byrne SM, Vreeland AC, Blaner WS, Noy N. Cross talk between signaling and vitamin A transport by the retinol-binding protein receptor STRA6. Mol Cell Biol. 2012;32: 3164–3175. doi:10.1128/MCB.00505-12

3. Silvaroli JA, Arne JM, Chelstowska S, Kiser PD, Banerjee S, Golczak M. Ligand Binding Induces Conformational Changes in Human Cellular Retinol-binding Protein 1 (CRBP1) Revealed by Atomic Resolution Crystal Structures. J Biol Chem. 2016;291: 8528–8540. doi:10.1074/jbc.M116.714535

4. Menozzi I, Vallese F, Polverini E, Folli C, Berni R, Zanotti G. Structural and molecular determinants affecting the interaction of retinol with human CRBP1. J Struct Biol. 2017;197: 330–339. doi:10.1016/j.jsb.2016.12.012

5. Folli C, Calderone V, Ottonello S, Bolchi A, Zanotti G, Stoppini M, et al. Identification, retinoid binding, and x-ray analysis of a human retinol-binding protein. Proc Natl Acad Sci U S A. 2001;98: 3710–3715. doi:10.1073/pnas.061455898

6. Moon RC. Comparative aspects of carotenoids and retinoids as chemopreventive agents for cancer. J Nutr. 1989;119: 127–134. doi:10.1093/jn/119.1.127

7. Dragnev KH, Rigas JR, Dmitrovsky E. The retinoids and cancer prevention mechanisms. The Oncologist. 2000;5: 361–368. doi:10.1634/theoncologist.5-5-361

bioRxiv preprint doi: https://doi.org/10.1101/2020.05.05.078410; this version posted May 5, 2020. The copyright holder for this preprint (which was not certified by peer review) is the author/funder. All rights reserved. No reuse allowed without permission.

8. Abramczyk H, Brozek-Pluska B. New look inside human breast ducts with Raman imaging. Raman candidates as diagnostic markers for breast cancer prognosis: Mammaglobin, palmitic acid and sphingomyelin. Anal Chim Acta. 2016;909: 91–100. doi:10.1016/j.aca.2015.12.038

9. Surmacki J, Brozek-Pluska B, Kordek R, Abramczyk H. The lipid-reactive oxygen species phenotype of breast cancer. Raman spectroscopy and mapping, PCA and PLSDA for invasive ductal carcinoma and invasive lobular carcinoma. Molecular tumorigenic mechanisms beyond Warburg effect. The Analyst. 2015;140: 2121–2133. doi:10.1039/c4an01876a

10. Abramczyk H, Brozek-Pluska B. Apical-basal polarity of epithelial cells imaged by Raman microscopy and Raman imaging: Capabilities and challenges for cancer research. J Mol Liq. 2017;245: 52–61. doi:10.1016/j.molliq.2017.05.142

11. Testerink N, Ajat M, Houweling M, Brouwers JF, Pully VV, van Manen H-J, et al. Replacement of retinyl esters by polyunsaturated triacylglycerol species in lipid droplets of hepatic stellate cells during activation. PloS One. 2012;7: e34945. doi:10.1371/journal.pone.0034945

12. Carotenoids: Nutrition, Analysis and Technology | Wiley. In: Wiley.com [Internet]. [cited 30 Oct 2019]. Available: https://www.wiley.com/en-us/Carotenoids%3A+Nutrition%2C+Analysis+and+Technology-p-9781118622261

13. Bender DA. Nutritional Biochemistry of the Vitamins by David A. Bender. In: Cambridge Core [Internet]. Sep 2003 [cited 30 Oct 2019]. doi:10.1017/CBO9780511615191

14. Micronutrients I of M (US) P on. Uses of Dietary Reference Intakes. National Academies Press (US); 2001. Available: https://www.ncbi.nlm.nih.gov/books/NBK222330/

15. Gottesman ME, Quadro L, Blaner WS. Studies of vitamin A metabolism in mouse model systems. BioEssays News Rev Mol Cell Dev Biol. 2001;23: 409–419. doi:10.1002/bies.1059

16. Napoli JL. Retinoic acid synthesis from beta-carotene in vitro. Methods Enzymol. 1993;214: 193–202. doi:10.1016/0076-6879(93)14066-r

17. Ong DE. Cellular retinoid-binding proteins. Arch Dermatol. 1987;123: 1693–1695a.

18. Ross AC, Ternus ME. Vitamin A as a hormone: Recent advances in understanding the actions of retinol, retinoic acid, and beta carotene. J Am Diet Assoc. 1993;93: 1285–1290. doi:10.1016/0002-8223(93)91956-Q

19. Chivot M. Retinoid therapy for acne. A comparative review. Am J Clin Dermatol. 2005;6: 13–19. doi:10.2165/00128071-200506010-00002

20. Love JM, Gudas LJ. Vitamin A, differentiation and cancer. Curr Opin Cell Biol. 1994;6: 825–831. doi:10.1016/0955-0674(94)90051-5

21. Niles RM. Signaling pathways in retinoid chemoprevention and treatment of cancer. Mutat Res Mol Mech Mutagen. 2004;555: 97–105. doi:10.1016/j.mrfmmm.2004.05.020

22. Stephensen CB. Vitamin a, Infection, and Immune Function*. Annu Rev Nutr. 2001;21: 167–192. doi:10.1146/annurev.nutr.21.1.167

bioRxiv preprint doi: https://doi.org/10.1101/2020.05.05.078410; this version posted May 5, 2020. The copyright holder for this preprint (which was not certified by peer review) is the author/funder. All rights reserved. No reuse allowed without permission.

23. Travis GH, Golczak M, Moise AR, Palczewski K. Diseases caused by defects in the visual cycle: retinoids as potential therapeutic agents. Annu Rev Pharmacol Toxicol. 2007;47: 469–512. doi:10.1146/annurev.pharmtox.47.120505.105225

24. Zouboulis CC. Retinoids – Which Dermatological Indications Will Benefit in the Near Future? Skin Pharmacol Physiol. 2001;14: 303–315. doi:10.1159/000056361

25. Doldo E, Costanza G, Agostinelli S, Tarquini C, Ferlosio A, Arcuri G, et al. Vitamin A, cancer treatment and prevention: the new role of cellular retinol binding proteins. BioMed Res Int. 2015;2015: 624627. doi:10.1155/2015/624627

26. Altucci L, Gronemeyer H. The promise of retinoids to fight against cancer. Nat Rev Cancer. 2001;1: 181–193. doi:10.1038/35106036

27. Siddikuzzaman null, Guruvayoorappan C, Berlin Grace VM. All trans retinoic acid and cancer. Immunopharmacol Immunotoxicol. 2011;33: 241–249. doi:10.3109/08923973.2010.521507

28. Niles RM. Use of Vitamins A and D in Chemoprevention and Therapy of Cancer: Control of Nuclear Receptor Expression and Function. Diet and Cancer: Molecular Mechanisms of Interactions. Boston, MA: Springer US; 1995. pp. 1–15. doi:10.1007/978-1-4899-0949-7_1

29. Arrieta O, González-De la Rosa CH, Aréchaga-Ocampo E, Villanueva-Rodríguez G, Cerón-Lizárraga TL, Martínez-Barrera L, et al. Randomized phase II trial of All-trans-retinoic acid with chemotherapy based on paclitaxel and cisplatin as first-line treatment in patients with advanced non-small-cell lung cancer. J Clin Oncol Off J Am Soc Clin Oncol. 2010;28: 3463–3471. doi:10.1200/JCO.2009.26.6452

30. Bryan M, Pulte ED, Toomey KC, Pliner L, Pavlick AC, Saunders T, et al. A pilot phase II trial of all-trans retinoic acid (Vesanoid) and paclitaxel (Taxol) in patients with recurrent or metastatic breast cancer. Invest New Drugs. 2011;29: 1482–1487. doi:10.1007/s10637-010-9478-3

31. Mawson AR. Retinoids in the treatment of glioma: a new perspective. Cancer Manag Res. 2012;4: 233–241. doi:10.2147/CMAR.S32449

32. Napoli JL. Cellular retinoid binding-proteins, CRBP, CRABP, FABP5: Effects on retinoid metabolism, function and related diseases. Pharmacol Ther. 2017;173: 19–33. doi:10.1016/j.pharmthera.2017.01.004

33. Acin-Perez R, Hoyos B, Zhao F, Vinogradov V, Fischman DA, Harris RA, et al. Control of oxidative phosphorylation by vitamin A illuminates a fundamental role in mitochondrial energy homoeostasis. FASEB J Off Publ Fed Am Soc Exp Biol. 2010;24: 627–636. doi:10.1096/fj.09-142281

34. Warburg O. On the Origin of Cancer Cells. Science. 1956;123: 309–314. doi:10.1126/science.123.3191.309

35. Singh A, Chatterjee S, Bansal P, Bansal A, Rawal S. Robot-assisted retroperitoneal lymph node dissection: Feasibility and outcome in postchemotherapy residual mass in testicular cancer. Indian J Urol IJU J Urol Soc India. 2017;33: 304–309. doi:10.4103/iju.IJU_8_17

36. Kwong J, Lo K-W, Chow LS-N, To K-F, Choy K-W, Chan FL, et al. Epigenetic silencing of cellular retinol-binding proteins in nasopharyngeal carcinoma. Neoplasia N Y N. 2005;7: 67–74. doi:10.1593/neo.04370

bioRxiv preprint doi: https://doi.org/10.1101/2020.05.05.078410; this version posted May 5, 2020. The copyright holder for this preprint (which was not certified by peer review) is the author/funder. All rights reserved. No reuse allowed without permission.

37. Noy N. Vitamin A Transport and Cell Signaling by the Retinol-Binding Protein Receptor STRA6. Subcell Biochem. 2016;81: 77–93. doi:10.1007/978-94-024-0945-1_3

38. Blaner WS. STRA6, a cell-surface receptor for retinol-binding protein: the plot thickens. Cell Metab. 2007;5: 164–166. doi:10.1016/j.cmet.2007.02.006

39. Goswami R, Kaplan MH. STAT Transcription Factors in T Cell Control of Health and Disease. Int Rev Cell Mol Biol. 2017;331: 123–180. doi:10.1016/bs.ircmb.2016.09.012

40. Imiela A, Polis B, Polis L, Abramczyk H. Novel strategies of Raman imaging for brain tumor research. Oncotarget. 2017;8: 85290–85310. doi:10.18632/oncotarget.19668

41. Abramczyk H, Surmacki J, Kopeć M, Olejnik AK, Lubecka-Pietruszewska K, Fabianowska-Majewska K. The role of lipid droplets and adipocytes in cancer. Raman imaging of cell cultures: MCF10A, MCF7, and MDA-MB-231 compared to adipocytes in cancerous human breast tissue. The Analyst. 2015;140: 2224–2235. doi:10.1039/c4an01875c

42. Abramczyk H, Surmacki J, Kopeć M, Olejnik AK, Kaufman-Szymczyk A, Fabianowska-Majewska K. Epigenetic changes in cancer by Raman imaging, fluorescence imaging, AFM and scanning near-field optical microscopy (SNOM). Acetylation in normal and human cancer breast cells MCF10A, MCF7 and MDA-MB-231. The Analyst. 2016;141: 5646–5658. doi:10.1039/c6an00859c

43. Liao C-S, Slipchenko MN, Wang P, Li J, Lee S-Y, Oglesbee RA, et al. Microsecond Scale Vibrational Spectroscopic Imaging by Multiplex Stimulated Raman Scattering Microscopy. Light Sci Appl. 2015;4. doi:10.1038/lsa.2015.38

44. Abramczyk H, Imiela A. The biochemical, nanomechanical and chemometric signatures of brain cancer. Spectrochim Acta A Mol Biomol Spectrosc. 2018;188: 8–19. doi:10.1016/j.saa.2017.06.037

45. Ji M, Orringer DA, Freudiger CW, Ramkissoon S, Liu X, Lau D, et al. Rapid, label-free detection of brain tumors with stimulated Raman scattering microscopy. Sci Transl Med. 2013;5: 201ra119. doi:10.1126/scitranslmed.3005954

46. Surmacki JM, Woodhams BJ, Haslehurst A, Ponder BAJ, Bohndiek SE. Raman micro-spectroscopy for accurate identification of primary human bronchial epithelial cells. Sci Rep. 2018;8: 1–11. doi:10.1038/s41598-018-30407-8

47. Reference database of Raman spectra of biological molecules - De Gelder - 2007 - Journal of Raman Spectroscopy - Wiley Online Library. [cited 30 Oct 2019]. Available: https://onlinelibrary.wiley.com/doi/abs/10.1002/jrs.1734

48. Mahadevan-Jansen A, Mitchell MF, Ramanujam N, Malpica A, Thomsen S, Utzinger U, et al. Near-infrared Raman spectroscopy for in vitro detection of cervical precancers. Photochem Photobiol. 1998;68: 123–132. doi:10.1562/0031-8655(1998)068<0123:nirsfv>2.3.co;2

49. Bozza PT, Viola JPB. Lipid droplets in inflammation and cancer. Prostaglandins Leukot Essent Fatty Acids. 2010;82: 243–250. doi:10.1016/j.plefa.2010.02.005

50. Stone N, Kendall C, Smith J, Crow P, Barr H. Raman spectroscopy for identification of epithelial cancers. Faraday Discuss. 2004;126: 141–157; discussion 169-183. doi:10.1039/b304992b

bioRxiv preprint doi: https://doi.org/10.1101/2020.05.05.078410; this version posted May 5, 2020. The copyright holder for this preprint (which was not certified by peer review) is the author/funder. All rights reserved. No reuse allowed without permission.

51. Thomas GJ. Raman spectroscopy of protein and nucleic acid assemblies. Annu Rev Biophys Biomol Struct. 1999;28: 1–27. doi:10.1146/annurev.biophys.28.1.1

52. Shaver JM, Christensen KA, Pezzuti JA, Morris MD. Structure of Dihydrogen Phosphate Ion Aggregates by Raman-Monitored Serial Dilution. Appl Spectrosc. 1998;52: 259–264.

53. Deng H, Bloomfield VA, Benevides JM, Thomas GJ. Dependence of the Raman signature of genomic B-DNA on nucleotide base sequence. Biopolymers. 1999;50: 656–666. doi:10.1002/(SICI)1097-0282(199911)50:6<656::AID-BIP10>3.0.CO;2-9

54. Guan Y, Choy GS-C, Glaser R, Thomas GJ. Vibrational Analysis of Nucleic Acids. 2. Ab Initio Calculation of the Molecular Force Field and Normal Modes of Dimethyl Phosphate. J Phys Chem. 1995;99: 12054–12062. doi:10.1021/j100031a039

55. Abramczyk H. Femtosecond primary events in bacteriorhodopsin and its retinal modified analogs: revision of commonly accepted interpretation of electronic spectra of transient intermediates in the bacteriorhodopsin photocycle. J Chem Phys. 2004;120: 11120–11132. doi:10.1063/1.1737731

56. Benador IY, Veliova M, Mahdaviani K, Petcherski A, Wikstrom JD, Assali E, et al. Mitochondria Bound to Lipid Droplets Have Unique Bioenergetics, Composition, and Dynamics That Support Lipid Droplet Expansion. Cell Metab. 2018;27: 869-885.e6. doi:10.1016/j.cmet.2018.03.003

57. Abramczyk H, Imiela A, Brożek-Płuska B, Kopeć M, Surmacki J, Śliwińska A. Aberrant Protein Phosphorylation in Cancer by Using Raman Biomarkers. Cancers. 2019;11: 2017. doi:10.3390/cancers11122017

58. Newcomer ME, Jones TA, Aqvist J, Sundelin J, Eriksson U, Rask L, et al. The three-dimensional structure of retinol-binding protein. EMBO J. 1984;3: 1451–1454.